Int. J. Heat Mass Transfer. Vol. 35, No. 7, pp. 1811–1821, 1992
Printed in Great Britain

0017–9310/92 $5.00 + 0.00

Numerical simulation and holographic visualization of double diffusive convection in a horizontal concentric annulus

J. DOSCH and H. BEER
Institut für Technische Thermodynamik, Technische Hochschule Darmstadt, Petersenstrasse 30, 6100 Darmstadt, Germany

(*Received* 8 *February* 1991)

Abstract—The time-dependent double diffusive convection in a horizontal concentric annulus is investigated both by numerical analysis and by holographic interferometry. In order to calculate stream functions, temperature-, concentration- and density-fields, the finite difference technique is utilized. Inner and outer cylinders of the annulus are kept isotherm, with the inner cylinder heated. The annulus is filled with an H_2O–NaCl solution, which is isothermal initially and submitted to a linear and stable stratification of the solution. The results reveal a considerable decrease in heat transfer as compared to natural convection without a stabilizing salt gradient. In addition experiments are performed on double diffusive convection about a vertical cylinder in a square container.

1. INTRODUCTION

Fluid flow phenomena under the simultaneous influence of concentration- and temperature-gradients have recently gained increased interest. In nature, flows in bodies of water are driven by the effects of temperature and concentration of dissolved materials and suspended particulate matter on density. Atmospheric flows can be initiated by temperature and water concentration differences. In technology some examples of flows driven by the simultaneous action of temperature and concentration gradients are drying processes, liquid gas storage, transpiration cooling and condensation in the presence of a non-condensing gas. Many aspects of material processing such as solidification and crystal growth entail such flows. Heat extraction out of the lower convecting zone in solar ponds is also influenced by double diffusive convection.

This paper is concerned with a numerical and experimental analysis of double diffusive convection in an annular gap between two isothermal concentric and horizontal cylinders. Additional experiments were performed on double diffusive convection about a horizontal heated cylinder in a square container with vertical side walls and the transferability was considered. The flow visualization was performed with the help of holographic interferometry.

In contrast to other geometries, double diffusive convection in a horizontal concentric annulus has not been investigated before. Heat transfer from a horizontal cylinder in a quiescent solutally stratified fluid, which is a related problem, was studied in the past by experiments only. Hubbell and Gebhart [1], as well as Neilson and Incropera [2], applied a constant overall heat flux. Because of a high conductive copper cylinder, the surface was isothermal but was changing its temperature with time. This experimental technique yielded overall heat transfer coefficients only. Neilson and Incropera [3] applied foil-heating which resulted in locally different surface temperatures. In this case local heat transfer coefficients could be determined. Flow visualization was performed by the shadowgraph imaging technique.

2. GOVERNING EQUATIONS AND SOLUTION PROCEDURE

Figure 1 depicts the geometry to be considered. The flow has been assumed to remain laminar, incompressible and two-dimensional, with constant fluid properties, except for the density change with temperature and salinity which gives rise to buoyancy forces. This results in the adoption of the Boussinesq approximation. For the numerical solution the flow is considered to be symmeric with respect to the vertical symmetric line.

The governing equations have been formulated with the stream function ψ', the temperature T', the vorticity ω' and the salinity c' as variables. In order to get dimensionless temperatures and concentrations, the difference between the temperatures of the hot and cold cylinder $(T'_h - T'_c)$ and the concentration difference between the bottom and the top of the gap, $(c'_b - c'_t)$, respectively, are used as references. For the numerical analysis the following dimensionless variables have been introduced, where the prime (′) indicates dimensional quantities:

NOMENCLATURE

A	geometry factor
c	concentration
d	diameter of inner cylinder
D	diameter of outer cylinder
Le	Lewis number
Nu	Nusselt number
Pr	Prandtl number
Ra_T, Ra_S	thermal and solutal Rayleigh numbers
s	gap width
S	dimensionless salinity
St	stability number, $St = Ra_S/Ra_T$
t	dimensionless time
u	dimensionless velocity
x	dimensionless coordinate.

Greek symbols

β	expansion coefficient
γ	angular coordinate
Γ	boundaries of computational plane
κ	thermal diffusivity
Λ	equivalent thermal conductivity
ν	kinematic viscosity
ψ	stream function
ω	vorticity.

Subscripts

b	bottom
c	cold, conduction
h	hot
i	inner
o	outer
S	solutal
T	thermal
t	top.

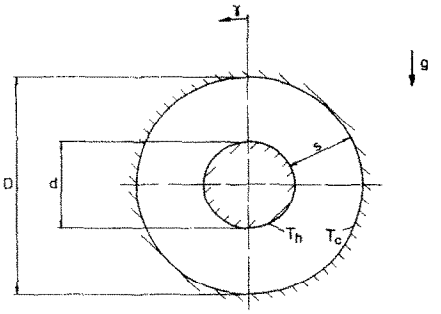

FIG. 1. Geometry of annulus.

$$x = x'/s; \quad t = t'\kappa/s^2; \quad u = u's/\kappa;$$
$$\psi = \psi'/\kappa; \quad \omega = \omega' s^2/\kappa;$$
$$T = \frac{T' - T'_c}{T'_h - T'_c}; \quad S = \frac{c' - c'_t}{c'_b - c'_t}. \tag{1}$$

In terms of these dimensionless variables the governing momentum, energy and mass equations in Cartesian coordinates are as follows:

$$\frac{\partial \omega}{\partial t} + \mathbf{u}\nabla\omega - Pr\,\nabla^2\omega = Pr\,Ra_T\left[\frac{\partial T}{\partial x} - A\,St\frac{\partial S}{\partial x}\right] \tag{2}$$

$$\frac{\partial T}{\partial t} + \mathbf{u}\nabla T - \nabla^2 T = 0 \tag{3}$$

$$\frac{\partial S}{\partial t} + \mathbf{u}\nabla S - \frac{1}{Le}\nabla^2 S = 0 \tag{4}$$

$$\nabla^2\psi = -\omega \tag{5}$$

$$\mathbf{u} = \nabla x\psi. \tag{6}$$

An important parameter will be the stability number St, which is defined as the ratio of the stabilizing forces due to the salinity gradient and the destabilizing forces caused by thermal buoyancy:

$$St = \frac{Ra_S}{Ra_T} = \frac{\beta_S(c'_b - c'_t)s}{\beta_T(T'_h - T'_c)D}. \tag{7}$$

Ra_T and Ra_S denote the modified Rayleigh numbers for temperature and salinity

$$Ra_T = \frac{g\beta_T(T'_h - T'_c)s^3}{\nu\kappa} \tag{8}$$

$$Ra_S = \frac{g\beta_S(c'_b - c'_t)s^4/D}{\nu\kappa} \tag{9}$$

where β_T and β_S are the thermal expansion coefficient and the solutal expansion coefficient, respectively. The geometry factor A is defined by the ratio of the diameter of the outer cylinder D and the gap width s.

To solve the governing equations in complex geometries, a numerical transformation method, such as that proposed by Thompson *et al.* [4], was applied (Fig. 2).

After the transformation of equations (2)–(5) into the computational rectangular plane (ξ, η plane), the boundary conditions for the vorticity transport equation (2) are those for rigid boundaries at Γ_1 and Γ_2 and $\omega = 0$ at the symmetric lines Γ_2, Γ_4. The stream function is constant, $\psi = 0$, at all boundaries. Temperatures are, $T = 1$ at the inner cylinder and $T = 0$ at the outer cylinder. The temperature gradient normal to the symmetric lines Γ_2, Γ_4 is zero, as well as the salt gradient normal to all boundaries.

Equations (2)–(5) and the boundary conditions are discretized with finite differences. All space derivatives can be represented by second-order central differences. The convective terms in equations (2) and (3) are writtten in divergence form, which guarantees a

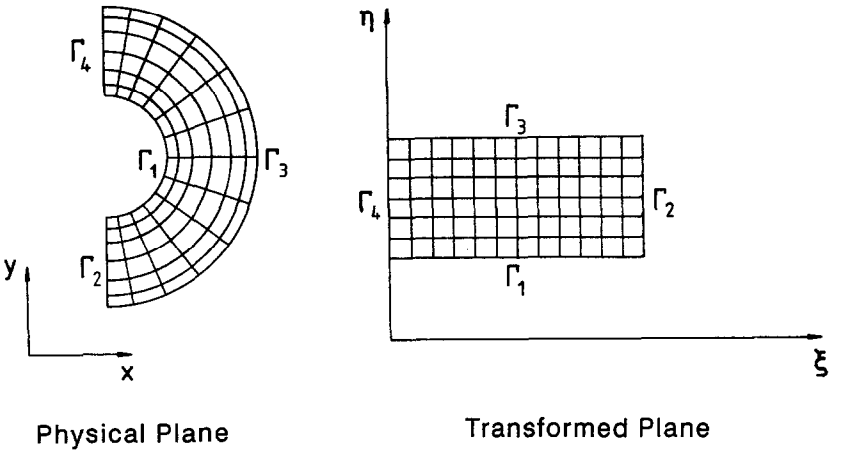

FIG. 2. Physical and transformed computational planes.

'wiggle-free' solution. Finally, the convective term in the species transport equation (4) is discretized using the second upwind method.

To solve the resulting linear equations, MSIP as an iterative method was applied. This technique, first developed by Schneider and Zedan [5], is an extension of the approach of Stone's [6] five-point formulation to a nine-point formulation.

In order to test the code a numerical analysis of natural convection without any salt gradient in a concentric horizontal annulus was performed. The results of these calculations show excellent agreement with the experimental findings of Kuehn and Goldstein [7].

3. EXPERIMENTS

The test apparatus (Fig. 3) consists of an outer copper ring (100 mm inner diameter) and a central copper tube of 40 mm diameter, respectively, between two Zerodur disks, thus forming a concentric annulus of 40 mm in length, which contains the stratified fluid. The transparent Zerodur-glass allows for holographic interferometry. Because of the very small thermal expansion coefficient of Zerodur, the refractive index is nearly independent of temperature. Through the outer copper ring as well as through the central tube, water acting as a heating or cooling fluid can be circulated, allowing the inner cylinder to be heated and the outer cylinder to be cooled. Thermocouples at the surface of both cylinders are installed to measure the surface temperatures T'_h and T'_c. The outer ring is fixed by side walls made of Plexiglas. In order to ensure a constant horizontal cross-section area in which the fluid rises during the filling process, the side walls are contoured as depicted in Fig. 3. To protect the copper surfaces from the corrosive saline

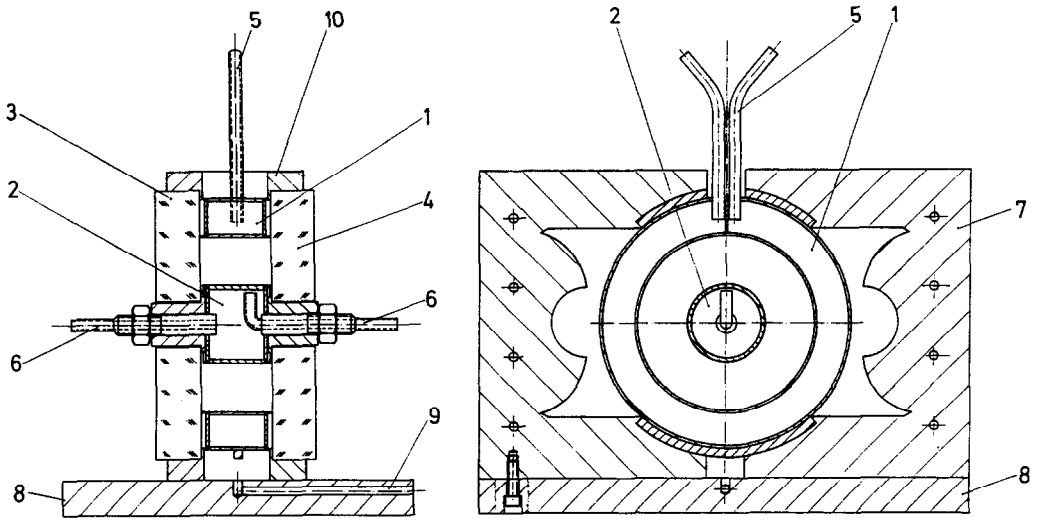

FIG. 3. Test apparatus: (1) outer copper ring; (2) inner copper cylinder; (3), (4) Zerodur disks; (5), (6) inlet and outlet tubes; (7) contoured Plexiglas side walls; (8) bottom plate; (9) filling tube; (10) flanges.

solution the cylinders were coated with a resistant lac.

A linear salinity profile was established by applying the double-bucket technique first proposed by Oster [8] to introduce continuously a progressively saltier solution at the bottom of the test cell. Experiments were performed with an H_2O–NaCl solution.

Holographic interferometry has been applied to visualize the complete and instantaneous field of refractive index in the test cell, without the necessity of disturbing the flow field by probes. A comparison of the measured field of the refractive index and that computed numerically verifies the numerical simulation. The refractive index was computed as a function of temperature and salinity as proposed by Ruddick and Shirtcliffe [9]. Confirmation of an initially linear salinity gradient was obtained by observing the interferogram of the isothermally salt stratified fluid in the annular gap before starting the experiment by heating the inner cylinder. The temperature difference between the inner and outer cylinder ranged from 1 K to 4 K, the salinity gradients varied from 0.16‰ cm^{-1} to 1.2‰ cm^{-1}.

4. RESULTS AND DISCUSSION

The analysis was performed for an H_2O–NaCl solution in the annular gap (annulus ratio $s/d = 0.75$, $d = 40$ mm) in the range $1.06 \leqslant St \leqslant 6.12$ and $4.0 \times 10^5 \leqslant Ra_T \leqslant 2.5 \times 10^6$. In order to demonstrate the influence of solute stratification on the formation of layered convection, the calculated stream-function, temperature and salinity are presented together with computed and experimental refractive indexes for comparison. Figure 4 depicts the numerical and experimental results for the dimensionless numbers $Ra_T = 8.84 \times 10^5$, $Ra_S = 1.48 \times 10^6$, $Pr = 6.59$ and $Le = 80$. According to its definition the stability number $St = Ra_S/Ra_T$ yields $St = 1.68$ in this case. The second column in Fig. 4 shows the numerical and experimental results at a time 120 s after heating of the inner cylinder started. Unlike the conditions in an unstratified fluid, the development of single convective layers is most evident. Layered convection starts at the top and bottom of the inner cylinder. The temperature field demonstrates the onset of convective heat transfer within the convective layers. However, heat conduction still dominates at the vertex. The salinity plots show the cellular structure of the flow by sharp interfaces between the convective layers. This flow structure originates from the ascent of solute-rich fluid along the cylinder when heating starts. As this fluid ascends, its density becomes progressively larger than that of the ambient. Sustained vertical motion is therefore inhibited by a negative buoyancy force, and the boundary layer is deflected horizontally. Density differences between the boundary layer and ambient fluid are intensified by the differential diffusion rates of heat and salt. Hence, the fluid begins to descend as it cools rapidly while retaining most of its salt. The foregoing process of layering is replicated, proceeding to the top of the cylinder. Various growing stages of the convecting layers are detectable by the salinity field. Computed and experimental fields of refractive index agree quite well, and place confidence in the numerical computation.

The third column shows the behaviour after a time of 300 s. At this time four convecting layers have developed around the inner cylinder and a horizontal propagation is evident. As the ascending flow is restored by vertical heat transfer from the lower vortices, the formation of boundary layer regions is intensified. As a result the convective heat transfer is increased and influences the temperature field around the inner cylinder. Only at the top and in particular at the bottom of the cylinder is the temperature distribution dominated by conduction. A proceeding equalization of salinity within the convecting layer characterizes the salinity field. Hence, steep salinity gradients appear across the interfaces between the layers. Numerical and experimental refractive indexes are in good agreement and confirm the numerical calculus.

In the fourth column of Fig. 4 the progress of stratification after 600 s is displayed. The fourth convecting layer has thickened and moved vertically upward. The flow is driven primarily by the heated cylinder, analogous to flow structures observed for side wall heating of a stable salinity gradient investigated by Wirtz *et al.* [10] and by Huppert *et al.* [11]. Convective heat transfer increases and dominates the temperature distribution in the annular gap on both sides of the cylinder. The gentle, downward slope of the interfaces is due to heat transfer from the warmer fluid below the interface to cooler fluid above it. A continuing equalization of salinity can be observed in the concentration plot. Again numerical and experimental refractive indexes agree well, with the exception of small differences in layer height at the third and fourth convective cells (from the bottom).

Finally, the fifth column shows results at a time of 1200 s after heating started. The growth of the convective motion has continued and nearly mixed conditions are achieved within each convective cell. At the top of the cylinder the measured field of refractive index deviates somewhat from the numerical results, though the agreement is good at the bottom. The deviation is caused by a stronger convective motion at the upper convective layers which erodes the interfaces much more in the numerical simulation than in the experiment. Although the number of grid points amounts to 181×91 the resolution at an interface with a steep salinity gradient is not sufficient. Hence, convective motion is able to erode the interfaces in computation more than in reality. This results in a falsified time scale if computation covers more than approximately 900 s. Nevertheless, the fundamental phenomena are represented quite well by the calculated plots.

The computed temperature distribution and the local temperature gradients, respectively, provide

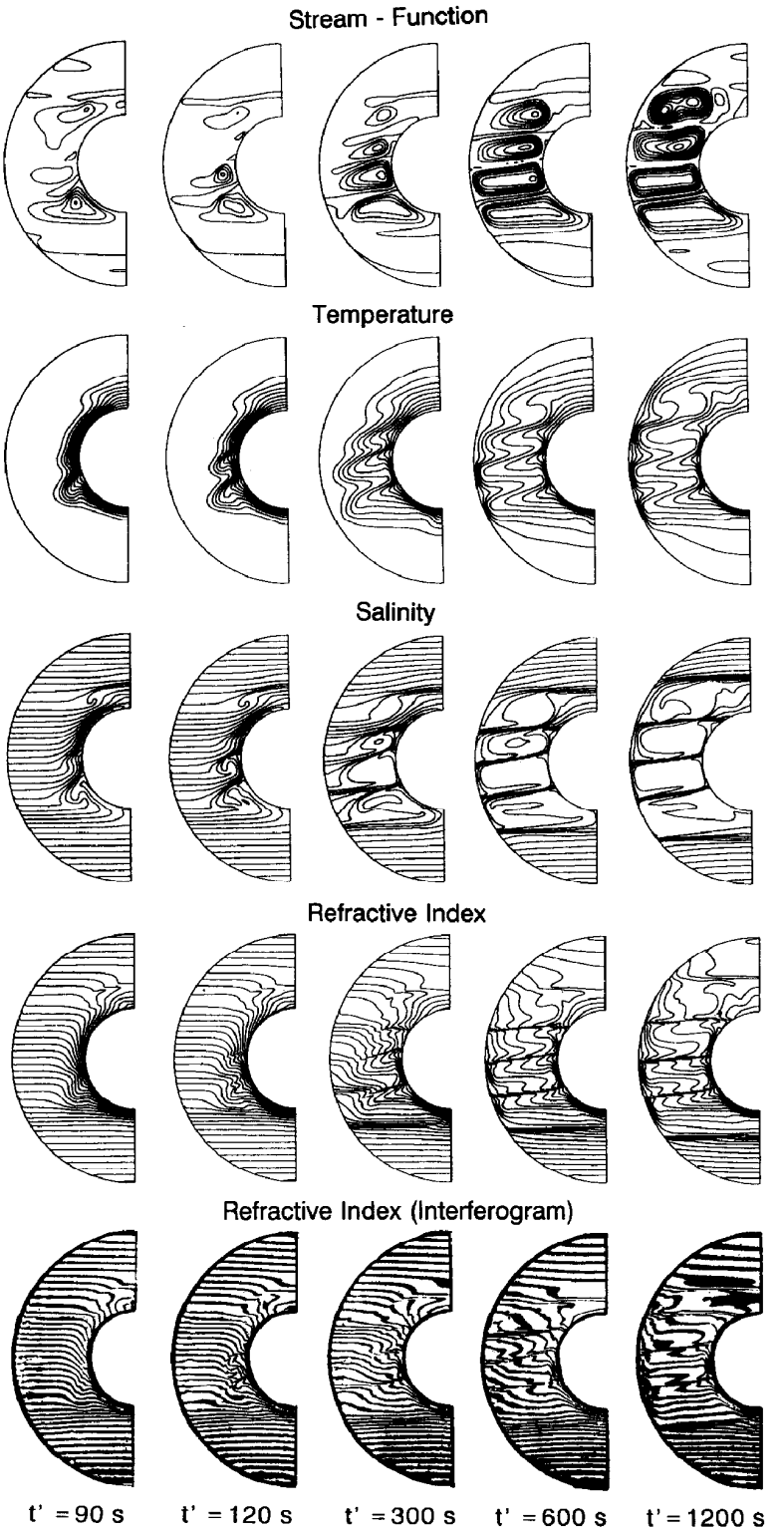

FIG. 4. Calculated and experimental results for double diffusive flow in an annular gap at various times: $Ra_T = 8.84 \times 10^5$; $St = 1.68$; $Pr = 6.59$; $Le = 80$.

detailed information about the local heat transfer at the inner and outer cylinder in the case of double diffusive convection. Heat transfer results are presented as local and average equivalent thermal conductivities Λ. This dimensionless parameter, which reflects the influence of convection on heat transfer is defined by

$$\Lambda = \frac{Nu}{Nu_c}, \quad Nu_{ci} = \frac{2s}{d \ln \frac{D}{d}}, \quad Nu_{co} = \frac{2s}{D \ln \frac{D}{d}} \tag{10}$$

where Nu is the actual Nusselt number based on the gap width s and Nu_c is the Nusselt number in the case of heat transfer solely by conduction. By integrating the local heat flux over the inner cylinder, one gets the average equivalent conductivity $\bar{\Lambda}_i$

$$\bar{\Lambda}_i = \frac{1}{\pi d} \int \Lambda \, \mathrm{d}l_i = \frac{\overline{Nu}}{Nu_{ci}} \tag{11}$$

where l_i denotes the arc length along the surface of the inner cylinder.

Figures 5–7 display local equivalent thermal conductivities at various times for the same set of parameters as in Fig. 4. The local equivalent conductivity along the inner cylinder at a time of 120 s is presented in Fig. 5 and makes evident the structure of the cellular flow. A strong enhancement of local heat transfer by the influence of fluid motion inside the growing convective cells can be observed at the bottom of the cylinder and at $\gamma = 105°$. Convection in the upper cells is less pronounced, resulting in only a slight deviation from the conduction solution ($\bar{\Lambda}_{ic} = 2.87$). As in the case of natural convection in an annular gap filled with an unstratified fluid, a minimum of the local equivalent conductivity occurs at the upper stagnation point of the inner cylinder.

Figure 6 shows the local equivalent thermal conductivity along the inner (solid line) and the outer (dashed line) cylinder at a time of 300 s. The influence of an increased cellular fluid motion on the local equivalent thermal conductivity is more pronounced than before. Mainly the two convecting layers at the bottom of the cylinder lead to local maxima. The circulating flow impinges on the inner cylinder, giving rise to large temperature gradients normal to the surface, which are the reason for the local maxima of the equivalent thermal conductivity. On the other hand, buoyancy forces at the top of the cylinder tend to deflect the fluid from the cylinder, leading to only a slight increase in heat transfer. Therefore, the enhancement of heat transfer is much smaller than at the bottom parts of the cylinder. In total the augmentation of the average equivalent thermal conductivity ($\bar{\Lambda}_i = 3.15$) has increased as compared to the conduction solution ($\bar{\Lambda}_{ic} = 1.95$). Heat transfer to the outer cylinder is negligible.

The local equivalent thermal conductivity after 1200 s is plotted in Fig. 7. Heat transfer is increased by the convective motion throughout the total cross-sectional area and maxima characterize the location of the convective cells. The convective layers have reached the surface of the outer cylinder by horizontal propagation and a distribution of Λ_a occurs, which is quite similar to that at the inner cylinder. The temperature gradients at the inner and outer cylinder are approximately the same in this case. As the heat flux density owing to steady heat conduction, however, is smaller at the outer cylinder, the equivalent conductivity adopts higher values at the outer cylinder.

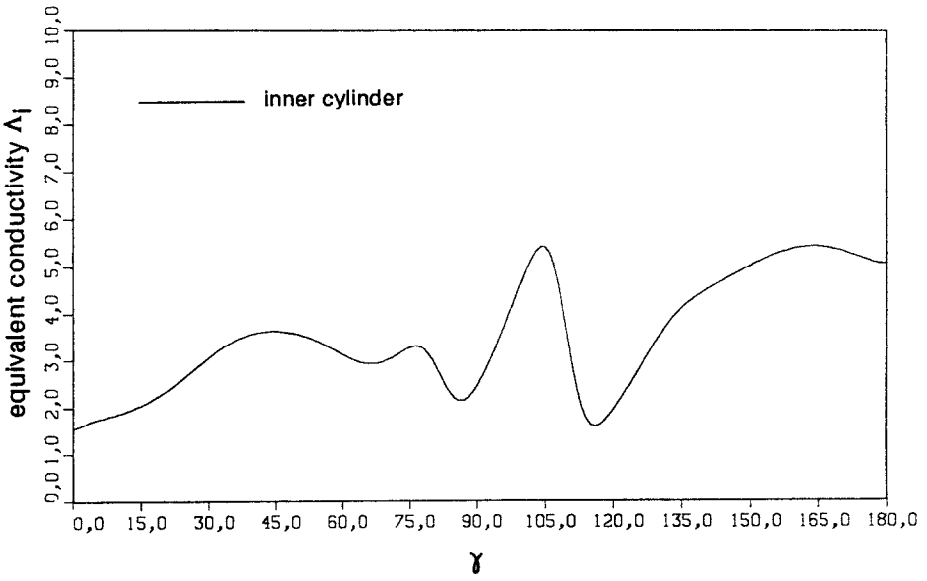

FIG. 5. Local equivalent thermal conductivity at the heated cylinder as a function of the angular coordinate γ; time $t' = 120$ s; $Ra_T = 8.84 \times 10^5$; $St = 1.68$.

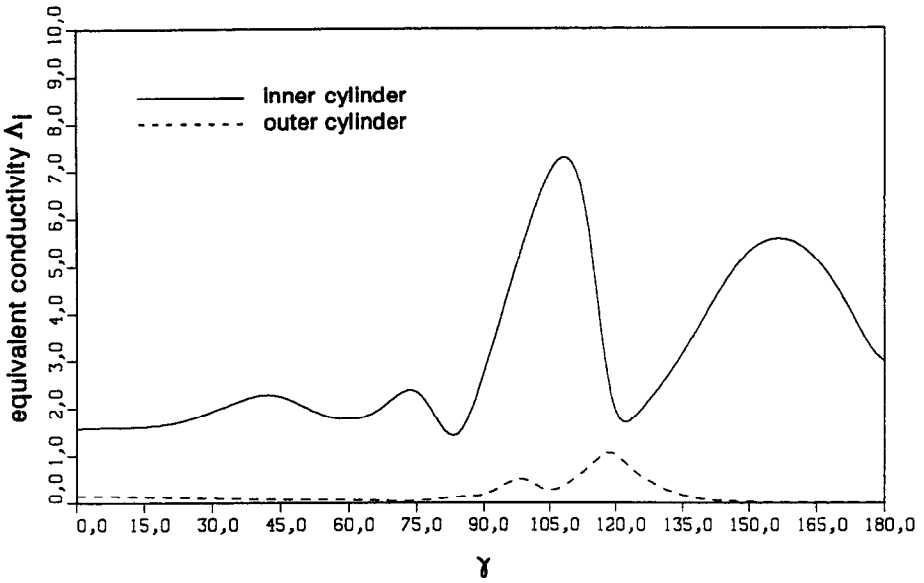

FIG. 6. Local equivalent thermal conductivity at the inner and outer cylinder as a function of the angular coordinate γ; time $t' = 300$ s; $Ra_T = 8.84 \times 10^5$; $St = 1.68$.

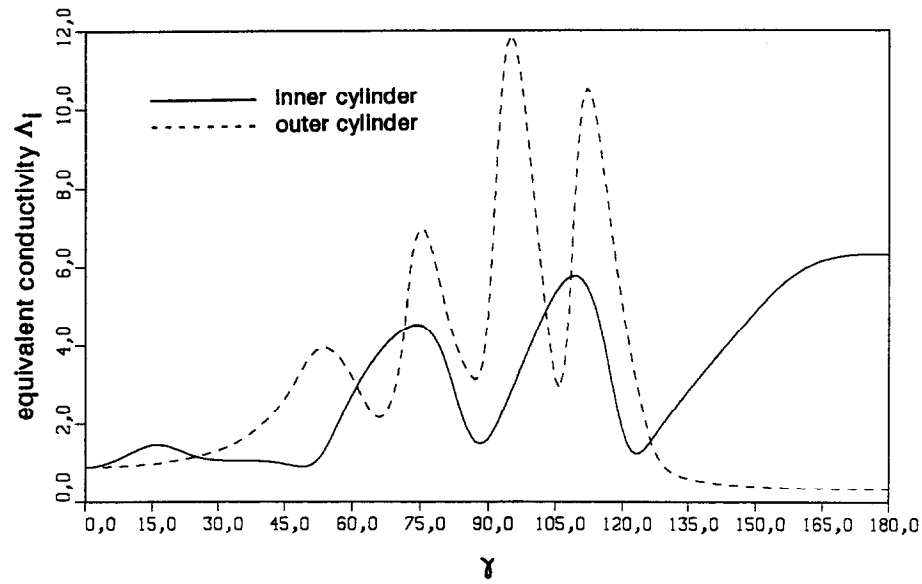

FIG. 7. Local equivalent thermal conductivity at the inner and outer cylinder as a function of the angular coordinate γ; time $t' = 1200$ s; $Ra_T = 8.84 \times 10^5$; $St = 1.68$.

In order to demonstrate the influence of various stratifications on heat transfer, the average equivalent thermal conductivity $\bar{\Lambda}_i$ at the inner cylinder is plotted as a function of dimensionless time for three different stability numbers, St, in Figs. 8(a)–(c). The conduction solution and the numerical solution for natural convection without solute stratification ($St = 0$) are displayed for comparison. In each case the sharp initial decrease of $\bar{\Lambda}_i$ is due to the conduction solution. The influence of solute stratification is revealed by comparing Figs. 8(a)–(c). As expected, strong stratification inhibits buoyancy driven flows around the cylinder, markedly reducing $\bar{\Lambda}_i$ as compared to an unstratified medium. Figure 8(a) shows a reduction of $\bar{\Lambda}_i$ to the values of mere conduction if the stability number is $St = 6.1$. In this case convective motion is fully suppressed by stratification. Only for a short time fluid motion occurs and increases the equivalent thermal conductivity $\bar{\Lambda}_i$ insignificantly but is rapidly damped by stabilizing salinity buoyancy forces. The temporal equivalent thermal conductivity for the case discussed in Fig. 4 is shown in Fig. 8(b). The stability

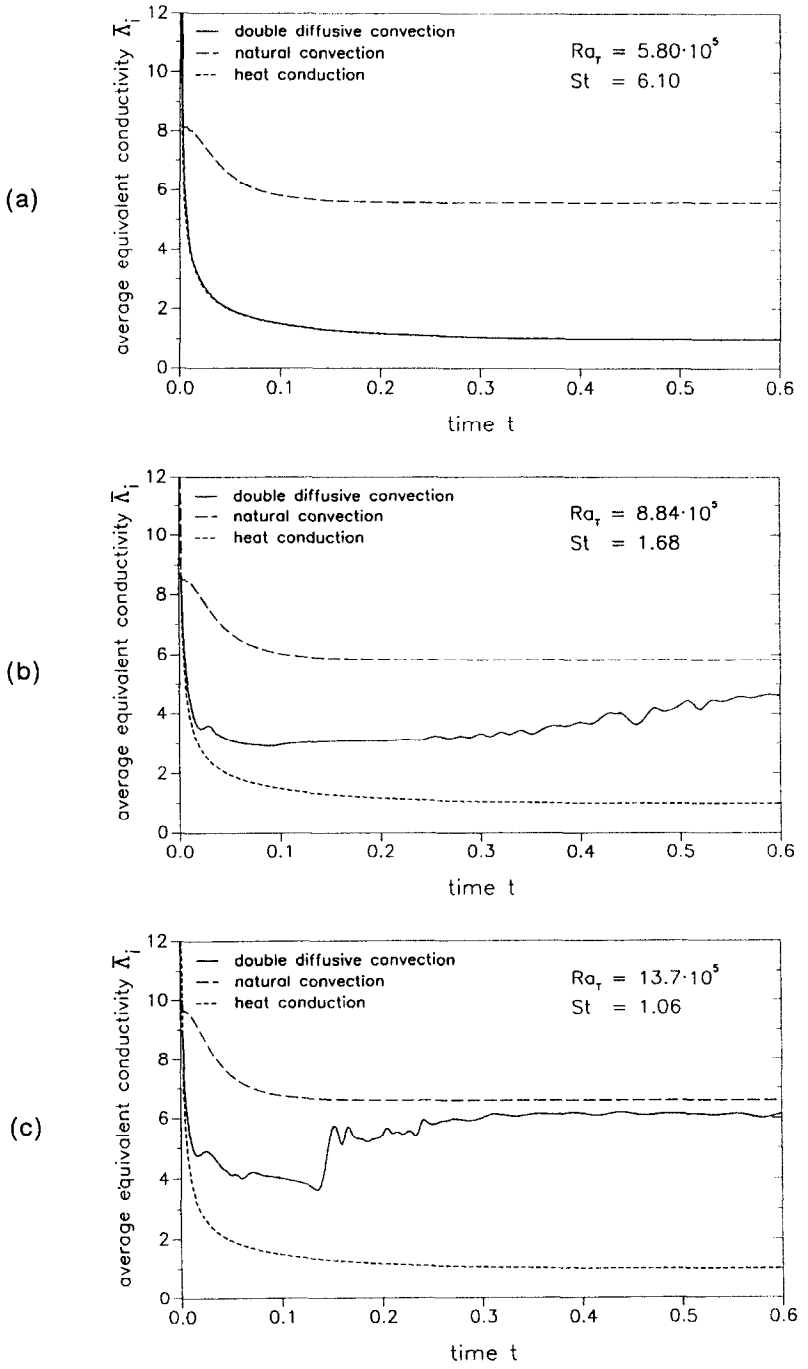

FIG. 8. Average equivalent thermal conductivity at the inner heated cylinder as a function of dimensionless time t ($t' = t \times 6200$ s).

number has decreased to $St = 1.68$. In contrast to Fig. 8(a), $\bar{\Lambda}_i$ increases in this case as double diffusive effects promote the formation and growth of convective layers in the annular gap on both sides of the cylinder. Development and a subsequent motion of interfaces cause an enhancement of $\bar{\Lambda}_i$ with time and finally the average equivalent conductivity approaches the value for an unstratified medium. Figure 8(c) shows the average equivalent thermal conductivity as a function of time for a stability number of $St = 1.06$. Diminishing stratification leads to an increased convective motion in the annular gap. After a short initial period of conduction dominated heat transfer, layered convection starts. Enhancement of convective heat trans-

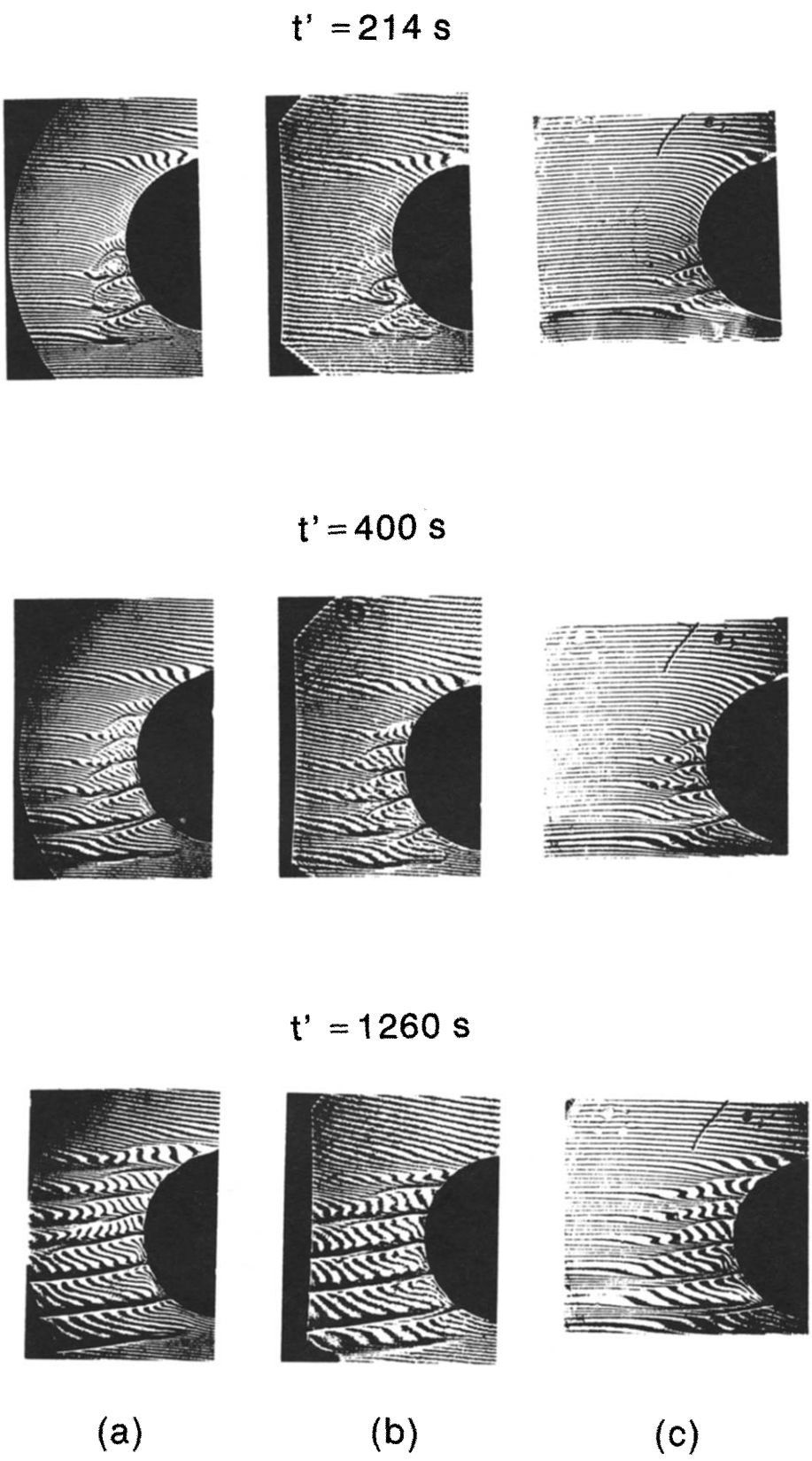

FIG. 9. Interferograms of double diffusive convection in an annular gap and around a cylinder in a container of two different widths.

fer occurs in accordance with the growth of convective layers. The experiments revealed that the height of the convective cells increases with decreasing stability number St. This fact was confirmed by Tanny and Tsinober [12] in side wall heating experiments. Hence, heat transfer increases with the aspect ratio of the convective layers. Subsequent erosion of the interfaces leads to a rearrangement of the convective layers and causes temporal fluctuations in $\bar{\Lambda}_i$ at advanced times. Finally, $\bar{\Lambda}_i$ approaches the conditions of heat transfer in an unstratified fluid.

The question arises whether the results obtained with double diffusive convection in a concentric annulus can be transferred to double diffusive convection at a heated horizontal cylinder with constant surface temperature. This cylinder is placed in the centre of a rectangular container with isothermal side walls, filled with the stably stratified solution. The distance between the side walls and the cylinder is chosen to be equal to and double the width of the previously investigated annulus. This allows for conclusions to be drawn upon the influence of the width of the container on the development of double diffusive convection around a horizontal cylinder. Figure 9 shows the experimental results for the three geometries investigated. The interferograms of double diffusive convection in a concentric annulus are compared with the results obtained in a rectangular container of two different widths at three different points in time. The column on the left shows the results for the concentric annulus and the two columns to the right depict the results with the horizontal cylinder in containers. Only the left half of the experimental set-up is shown. The most important dimensionless numbers are listed in Table 1. For better comparability the characteristic length was set equal to the width of the annulus.

The first row shows the interferograms at a time $t' = 214$ s after heating of the cylinder started. There is no evident difference between the three geometries as the onset of cellular convection is restricted to the fluid in the vicinity of the heated cylinder. Hence the geometry of the outer cylinder and the side walls of the container, respectively, are of minor influence. No cellular convection can be observed at the top of the cylinders.

The second row shows the interferograms after $t' = 400$ s. Layered convection starts at the bottom of the cylinder and some additional convecting layers have developed around the lower part of the cylinder in all three geometries investigated. However, in the wide container convection has not yet started at the top of the cylinder. The reason is the slightly smaller thermal Rayleigh number for this geometry.

In the third row the experimental results after $t' = 21$ min are presented. In the annular gap and in the narrrow container cellular convection covers the whole area between the inner and outer cylinder and between the cylinder and the side walls, respectively. Cellular convection is driven by temperature gradients in the vicinity of the inner cylinder and the outer surfaces. In the wide container convective motion has not yet reached the outer wall. Convection is only driven by one steep temperature gradient near the inner cylinder. As cellular convection proceeds to the outer surface of this container, the aspect ratio of the convection cells decreases steadily. Therefore, convection in this wide container is less pronounced than in the narrow geometries.

This allows the conclusion that experimental and numerical results obtained for cellular convection in an annular gap may be transferred to a cylinder in a container only for times preceding the contact of the cells with the outer gap wall. Later on the convective motion in the concentric annulus is more intense than around the cylinder in a wide container. If the distance between the cylinder and a vertical side wall equals the gap width of a concentric annulus, no essential differences occur.

Table 1

	Ra_S	Ra_T	St
Concentric annulus	4.1×10^5	11.4×10^5	3.61
Narrow container	27.7×10^5	8.1×10^5	3.42
Wide container	31.6×10^5	7.7×10^5	3.59

5. CONCLUSIONS

The object of the present numerical and experimental analysis is the investigation of stabilizing effects due to solute gradients on the flow in an annular gap and on heat transfer between isothermal inner and outer cylinders. The nature of the flow and the heat transfer depend strongly on the stability number, St, which relates the stabilizing effect of salt concentration gradient to the destabilizing thermal buoyancy. For large values of St, the convective motion around the heated cylinder is largely suppressed and, therefore, heat transfer is dominated by conduction. With decreasing stability number multiple convective layers develop around the heated cylinder. The layers are separated by diffusive interfaces, and the recirculating flow within each layer is driven by the temperature gradient between the inner and the outer cylinder. The height of the convective layers increases with diminishing stability number and the convective heat transport is enhanced. Local equivalent thermal conductivities are presented as a function of time and reveal the influence of layered convection on heat transfer. Average equivalent thermal conductivities vary strongly with time and depend on the magnitude of St. The results of numerical investigation agree well with experimental findings.

Experiments reveal that the results for cellular convection in a concentric annulus may be transferred to cellular convection about a horizontal cylinder in a container with vertical walls as long as the cellular convection does not reach the outer wall.

Acknowledgement—The support of this work by the Deutsche Forschungsgemeinschaft is greatly acknowledged.

REFERENCES

1. R. H. Hubbell and B. Gebhart, Transport processes induced by a heated horizontal cylinder submerged in quiescent salt-stratified water, *Proc. 24th Heat Transfer and Fluid Mechanics Institute*, pp. 203–219 (1974).
2. D. G. Neilson and F. P. Incropera, Double-diffusive flow and heat transfer for a cylindrical source submerged in a salt-stratified solution, *Int. J. Heat Mass Transfer* **30**, 2559–2570 (1987).
3. D. G. Neilson and F. P. Incropera, Local heat transfer from a horizontal cylinder in unstratified and salt-stratified fluid layers, *Int. J. Heat Mass Transfer* **31**, 660–663 (1988).
4. J. F. Thompson, Z. U. A. Warsi and C. W. Mastin, Boundary fitted coordinate systems for numerical solution of partial differential equations—a review, *J. Comput. Phys.* **47**, 1–108 (1982).
5. G. E. Schneider and M. Zedan, A modified strongly implicit procedure for the numerical solution of field problems, *Numer. Heat Transfer* **4**, 1–19 (1981).
6. H. L. Stone, Iterative solution of implicit approximations of multidimensional partial differential equations, *SIAM J. Numer. Analysis* **5**, 530–558 (1968).
7. T. H. Kuehn and R. J. Goldstein, An experimental and theoretical study of natural convection in the annulus between horizontal concentric cylinders, *J. Fluid Mech.* **74**, 695–719 (1976).
8. G. Oster, Density gradients, *Scient. Am.* **213**, 70–76 (1965).
9. B. R. Ruddick and T. G. L. Shirtcliffe, Data for double-diffusers: physical properties of aqueous salt–sugar solutions, *Deep Sea Res.* **26A**, 775–787 (1979).
10. R. A. Wirtz, D. G. Briggs and C. F. Chen, Physical and numerical experiments on layered convection in a density-stratified fluid, *Geophys. Fluid Dyn.* **3**, 265–288 (1972).
11. H. E. Huppert, R. C. Kerr and M. A. Hallworth, Heating or cooling a stable compositional gradient from the side, *Int. J. Heat Mass Transfer* **27**, 1395–1401 (1984).
12. J. Tanny and A. B. Tsinober, The dynamics and the structure of double-diffusive layers in sidewall-heating experiments, *J. Fluid Mech.* **196**, 135–156 (1988).

SIMULATION NUMERIQUE ET VISUALISATION HOLOGRAPHIQUE DE LA CONVECTION DOUBLE DIFFUSIVE DANS UN ANNEAU HORIZONTAL ET CONCENTRIQUE

Résumé—Le développement temporel de la convection double diffusive dans un anneau horizontal et concentrique a été étudié aussi bien numériquement qu' expérimentalement par interférométrie holographique. La fonction de courant et les champs de température, de concentration et de densité ont été calculés par le procédé numérique des différences finies. L'anneau était rempli d'une solution H_2O–NaCl initialement isotherme et á concentration stratifiée stable. Les parois cylindriques externe et interne étaient maintenues á température constante, le cylindre interne étaut chauffé. Les résultats montrent une diminution considérable de transfert de chaleur en comparaison à la convection naturelle sans gradients de sel stabilisants. De plus, des essais expérimentaux de convection double diffusive ont été réalisés à l'extérieur d'un cylindre horizontal chauffé et placé dans un récipient rectangulaire à parois latérales verticales.

NUMERISCHE BERECHNUNG UND HOLOGRAPHISCHE VISUALISIERUNG DER DOPPELT DIFFUSIVEN KONVEKTION IN EINEM HORIZONTALEN, KONZENTRISCHEN RINGSPALT

Zusammenfassung—Die zeitliche Entwicklung der doppelt diffusiven Konvektion in einem horizontalen konzentrischen Ringspalt wurde sowohl numerisch als auch mit Hilfe der holographischen Interferometrie untersucht. Zur Berechnung der Stromfunktion, der Temperatur-, Konzentrations- und Dichte-Felder wurde das Finite Differenzen Verfahren angewandt. Der Ringspalt war mit einer anfänglich isothermen und stabil konzentrationsgeschichteten H_2O–NaCl-Lösung gefüllt. Äußerer und innerer Zylinder wurden isotherm gehalten, der innere Zylinder war beheizt. Die Ergebnisse offenbaren eine beträchtliche Abnahme der Wärmeübertragung verglichen mit natürlicher Konvektion ohne stabilisierenden Salzgradienten. Zusätzlich sind Experimente zur doppelt diffusiven Konvektion um einen horizontalen beheizten Zylinder in einen rechteckigen Behälter mit vertikalen Seitenwänden durchgeführt worden.

ЧИСЛЕННОЕ МОДЕЛИРОВАНИЕ И ГОЛОГРАФИЧЕСКАЯ ВИЗУАЛИЗАЦИЯ ДИФФУЗИОННОЙ ТЕПЛОВОЙ И КОНЦЕНТРАЦИОННОЙ КОНВЕКЦИИ В ГОРИЗОНТАЛЬНОМ КОНЦЕНТРИЧЕСКОМ ЗАЗОРЕ

Аннотация—С помощью численного анализа и голографической интерферометрии исследуется нестационарная диффузионная, тепловая и концентрационная конвекция в горизонтальном концентрическом зазоре. Для расчета функций тока, полей температуры, концентрации и плотности используется метод конечных разностей. Внутренний и внешний цилиндры являются изотермическими, тепловой поток подводится к внутреннему цилиндру. Зазор заполнен раствором H_2O–NaCl, который изначально является изотермическим, а затем подвергается линейной и устойчивой стратификации. Результаты свидетельствуют о значительном снижении интенсивности теплопереноса по сравнению с естественной конвекцией при отсутствии стабилизирующего градиента солёности. Кроме того, были проведены эксперименты по диффузионной, тепловой и концентрационной конвекции у вертикального цилиндра, расположенного в квадратном контейнере.